Supporting Information

Synthesis and self-assembly of aminyl and alkynyl substituted sophorolipids

Abdoul Aziz Ba,[a] Jonas Everaert,[b] Alexandre Poirier,[a] Patrick Le Griel,[a] Wim Soetaert,[c] Sophie L. K. W. Roelants,[c] Daniel Hermida-Merino,[d] Christian V. Stevens,[b] Niki Baccile[a,*]

[a] Sorbonne Université, Centre National de la Recherche Scientifique, Laboratoire de Chimie de la Matière Condensée de Paris, LCMCP, F-75005 Paris, France

[b] SynBioC, Department of Green Chemistry and Technology, Ghent University, Ghent, Belgium

[c] InBio, Department of Biotechnology, Ghent University, Ghent, Belgium

[d] Netherlands Organisation for Scientific Research (NWO), DUBBLE@ESRF BP CS40220, 38043 Grenoble, France

Synthesis procedure, ^{1}H and ^{13}C NMR analyses of modified sophorolipids

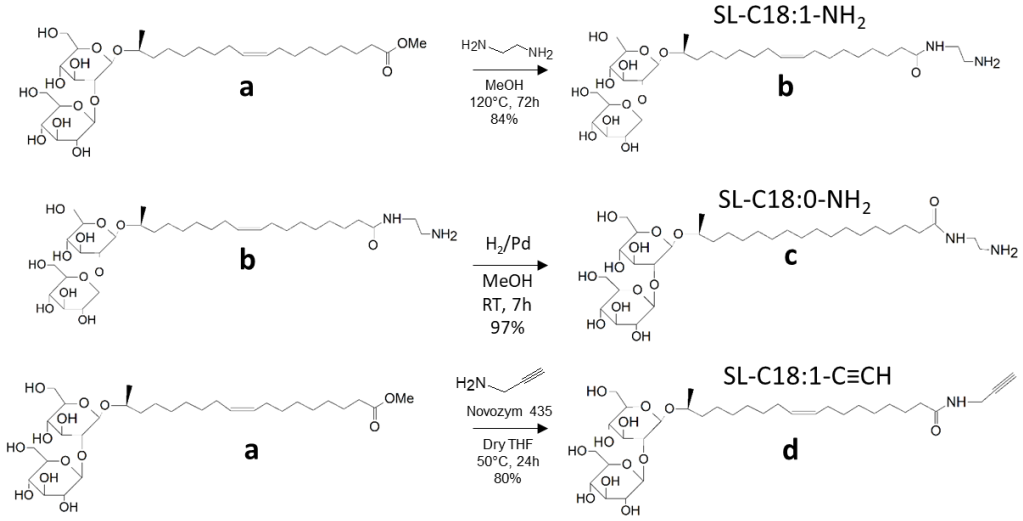

Figure S 1 – Synthesis conditions for aminyl and alkynyl sophorolipids. (a) Monounsaturated sophorolipids methyl ester, SL-C18:1-OMe, prepared from a previous study.[1] (b) Monounsaturated aminyl sophorolipid, SL-C18:1-NH_2. (c) Saturated aminyl sophorolipid, SL-C18:0-NH_2. (d) Monounsaturated alkynyl sophorolipid, SL-C18:1-C≡CH.

Monounsaturated sophorolipid methyl ester, SL-C18:1-OMe (Figure S 1a). *SL-C18:1-OMe* is prepared according to a previous study[1] from lactonic sophorolipids (LSL)[1] and following a literature process[2,3] In a 100 mL round-bottom flask, sodium methylate is formed *in situ* by adding 0.083 g of sodium (3.63 mmol, 0.5 eq) to 20 mL of anhydrous MeOH and 5 g of LSL (7.26 mmol). The flask is equipped with a reflux condenser and a tube containing $CaCl_2$ to protect the reaction mixture from atmospheric humidity. The reaction mixture is stirred for 3 hours at reflux temperature, cooled to room temperature and acidified to neutral pH with acetic acid. The mixture was concentrated under reduced pressure, dissolved in deionized water and cooled to 0°C in an ice bath. The sophorolipid methyl ester (**b**) precipitates as a white powder. The precipitate is filtered, washed with water and dried under reduced pressure (79%, 3.65 g). The molecule in Figure S 1**a** is identified by ^{1}H and ^{13}C NMR (Figure S 2). The allocation of the peaks is in agreement with the data relating to this compound.[3]

Monounsaturated aminyl sophorolipid, SL-C18:1-NH_2 (Figure S 1**b**): in a 50 mL pressurized oven-dried bottle, 2 g of (**a**) (3.14 mmol, 1 eq) is dissolved in 12 mL of anhydrous MeOH, to which 2.12 ml of ethylenediamine (31.4 mmol, 10 equivalents, 1.89 g) is added. The reaction mixture is heated at 120°C for 72 hours with magnetic stirring. The reaction is followed by NMR analysis until complete conversion. The solvent of the reaction mixture is evaporated *in vacuo* and the product is purified by chromatography on silica gel (10% H_2O, 25% MeOH,

15% Et_3N, 50% EtOAc). The desired product is obtained in the form of a viscous brown oil (84%, 1.75 g) and identified by ^1H and ^{13}C NMR. Attributions of the ^1H and ^{13}C NMR signals are given below. The corresponding ^1H NMR spectrum is given in Figure S 3.

^1H NMR (400 MHz, MeOD-d4): δ = 1.25 (3H, d, *J*=6.2 Hz, C$\underline{H}_3$CH), 1.29-1.48 (17H, m, C$\underline{H}_a$H$_b$CHCH$_3$, 8xC$\underline{H}_2$(CH$_2$)$_2$), 1.58-1.65 (3H, m, CH$_a\underline{H}_b$CHCH$_3$, C$\underline{H}_2$CH$_2$CONH), 2.02-2.08 (4H, m, 2xC$\underline{H}_2$CH=CH), 2.19 (2H, t, *J*=7.5 Hz, C$\underline{H}_2$CONH), 2.89 (2H, t, *J*=6.1 Hz, C$\underline{H}_2$NH$_2$), 3.21-3.41 (8H, m, 6xC$\underline{H}$OC, CONHC$\underline{H}_2$), 3.45 (1H, dxd, *J*=8.4 Hz, *J*=8.4 Hz, C$\underline{H}$OC), 3.56 (1H, dxd, *J*=8.7 Hz, *J*=8.7 Hz, C$\underline{H}$OC), 3.63-3.69 (2H, m, 2xC$\underline{H}_a$H$_b$OH), 3.79-3.89 (3H, m, 2xCH$_a\underline{H}_b$OH, $\underline{C}$HCH$_3$), 4.45 (1H, d, *J*=7.7 Hz, C$\underline{H}$(O)$_2$), 4.64 (1H, d, *J*=7.8 Hz, C$\underline{H}$(O)$_2$), 5.34- 5.38 (2H, m, C$\underline{H}$=C$\underline{H}$). **^{13}C NMR (100.6 MHz, MeOD-d4):** δ = 21.9 ($\underline{C}$H$_3$CH), 26.2 ($\underline{C}$H$_2$(CH$_2$)$_2$), 26.8 ($\underline{C}$H$_2$CH$_2$CONH), 28.1 (2x$\underline{C}$H$_2$CH=CH), 30.2 ($\underline{C}$H$_2$(CH$_2$)$_2$), 30.3 (2x$\underline{C}$H$_2$(CH$_2$)$_2$), 30.4 ($\underline{C}$H$_2$(CH$_2$)$_2$), 30.8 (2x$\underline{C}$H$_2$(CH$_2$)$_2$), 30.9 ($\underline{C}$H$_2$(CH$_2$)$_2$), 37.0 ($\underline{C}$H$_2$CONH), 37.8 ($\underline{C}$H$_2$CHCH$_3$), 40.4 (CONH$\underline{C}$H$_2$), 41.4 ($\underline{C}$H$_2$NH$_2$), 62.7 ($\underline{C}$H$_2$OH), 63.1 ($\underline{C}$H$_2$OH), 71.5 ($\underline{C}$HOC), 71.8 ($\underline{C}$HOC), 75.9 ($\underline{C}$HOC), 77.8 (2x$\underline{C}$HOC), 78.2 ($\underline{C}$HOC), 78.3 ($\underline{C}$HOC), 78.9 ($\underline{C}$HCH$_3$), 81.9 ($\underline{C}$HOC), 102.7 ($\underline{C}$H(O)$_2$), 104.7 ($\underline{C}$H(O)$_2$), 130.8 (CH=$\underline{C}$H), 130.9 ($\underline{C}$H=CH), 177.2 ($\underline{C}$ONH).

Saturated aminyl sophorolipid, *SL-C18:0-NH$_2$* (Figure S 1**c**): 1.75 g of **b** is dissolved in 30 mL of MeOH under an argon atmosphere and to which 175 mg (10% w/w) of Pd/C (10%) is added. The reaction mixture is stirred for 7 hours under an atmosphere of 5 bars of H_2, after which it is filtered through celite. After removing the solvent under vacuum, a white solid of saturated aminyl sophorolipid is obtained (1.70 g, 97% yield), as identified by the loss of the C$\underline{H}$=C$\underline{H}$ peak at 5.37 ppm in solution ^1H NMR, as reported for a similar reaction on acidic sophorolipids.[4,5]

Monounsaturated alkynyl sophorolipid, *SL-C18:1-C≡CH* (Figure S 1**d**): in a dried 50 mL flask, 1.8 g of (**a**) (3.14 mmol, 1 eq) is dissolved in 30 mL of anhydrous THF. 0.6 g of Novozym 435 (33% by weight of sophorolipid) and 361 µL of propargylamine (5.65 mmol, 2 equivalents, 0.311 g) are added and the reaction mixture is heated at 50°C for 24 hours under magnetic stirring. The reaction is followed by NMR until complete conversion. The reaction mixture is filtered through a sintered glass filter and the solvent is evaporated *in vacuo*. The product is purified by chromatography on silica gel (5% H_2O, 20% MeOH, 75% EtOAc). The desired product is obtained in the form of a yellowish powder (80%, 1.5 g). Attributions of the

^{1}H and ^{13}C NMR signals are given below. The corresponding ^{1}H NMR spectrum is given in Figure S 4.

^{1}H NMR (400 MHz, MeOD-d4): δ = 1.25 (3H, d, *J*=6.3 Hz, C$\underline{H}_3$CH), 1.30-1.49 (17H, m, C$\underline{H}_a$H$_b$CHCH$_3$, 8xC$\underline{H}_2$(CH$_2$)$_2$), 1.56-1.65 (3H, m, CH$_a\underline{H}_b$CHCH$_3$, C$\underline{H}_2$CH$_2$CONH), 2.03-2.04 (4H, m, 2xC$\underline{H}_2$CH=CH), 2.19 (2H, t, *J*=7.5 Hz, C$\underline{H}_2$CONH), 2.56 (1H, t, *J*=2.5 Hz, C≡C$\underline{H}$), 3.21-3.33 (5H, m, 5xC$\underline{H}$OC), 3.37 (1H, dxd, *J*=8.9 Hz, *J*=8.9 Hz, C$\underline{H}$OC), 3.45 (1H, m, C$\underline{H}$OC), 3.55 (1H, dxd, *J*=8.7 Hz, *J*=8.7 Hz, C$\underline{H}$OC), 3.63-3.68 (2H, m, 2xC$\underline{H}_a$H$_b$OH), 3.79-3.88 (3H, m, 2xCH$_a\underline{H}_b$OH, $\underline{C}$HCH$_3$), 3.94 (2H, d, *J*=2.5 Hz, NHC$\underline{H}_2$C≡C), 4.45 (1H, d, *J*=7.7 Hz, C$\underline{H}$(O)$_2$), 4.64 (1H, d, *J*=7.8 Hz, C$\underline{H}$(O)$_2$), 5.34- 5.37 (2H, m, C$\underline{H}$=C$\underline{H}$). **^{13}C NMR (100.6 MHz, MeOD-d4):** δ = 21.9 ($\underline{C}$H$_3$CH), 26.2 ($\underline{C}$H2(CH$_2$)$_2$), 26.9 ($\underline{C}$H$_2$CH$_2$CONH), 28.1 ($\underline{C}$H$_2$CH=CH), 28.2 ($\underline{C}$H$_2$CH=CH), 29.4 (NH$\underline{C}$H$_2$C≡C), 30.2 (2x$\underline{C}$H$_2$(CH$_2$)$_2$), 30.3 ($\underline{C}$H$_2$(CH$_2$)$_2$), 30.4 ($\underline{C}$H$_2$(CH$_2$)$_2$), 30.8 ($\underline{C}$H$_2$(CH$_2$)$_2$), 30.8 ($\underline{C}$H$_2$(CH$_2$)$_2$), 30.9 ($\underline{C}$H$_2$(CH$_2$)$_2$), 36.8 ($\underline{C}$H$_2$CONH), 37.8 ($\underline{C}$H$_2$CHCH$_3$), 62.8 ($\underline{C}$H$_2$OH), 63.1 ($\underline{C}$H$_2$OH), 71.5 ($\underline{C}$HOC), 71.8 ($\underline{C}$HOC), 72.0 (C≡$\underline{C}$H), 75.9 ($\underline{C}$HOC), 77.8 (2x$\underline{C}$HOC), 78.2 ($\underline{C}$HOC), 78.3 ($\underline{C}$HOC), 78.9 ($\underline{C}$HCH$_3$), 80.7 ($\underline{C}$≡CH), 81.9 ($\underline{C}$HOC), 102.7 ($\underline{C}$H(O)$_2$), 104.7 ($\underline{C}$H(O)$_2$), 130.8 (CH=$\underline{C}$H), 130.9 ($\underline{C}$H=CH), 175.9 ($\underline{C}$ONH).

Solution Nuclear Magnetic Resonance (*NMR*): ^{1}H NMR and ^{13}C NMR spectra were recorded at 25 °C at 400 MHz and 100.6 MHz, respectively using a Bruker AVANCE III HD 400 Nanobay spectrometer, equipped with 1H/BB z-gradient probe (BBO, 5 mm). Chemical shifts (δ) are reported in parts per million (ppm) relative to tetramethylsilane (δ = 0) and referenced to the residual solvent peak (MeOD-d4 δ_H = 3.31 and δ_C = 49.0). All spectra were processed using TOPSPIN 3.2. ^{1}H, ^{13}C (APT), COSY, HSQC and HMBC NMR spectra were acquired through the standard sequences available in the Bruker pulse program library.

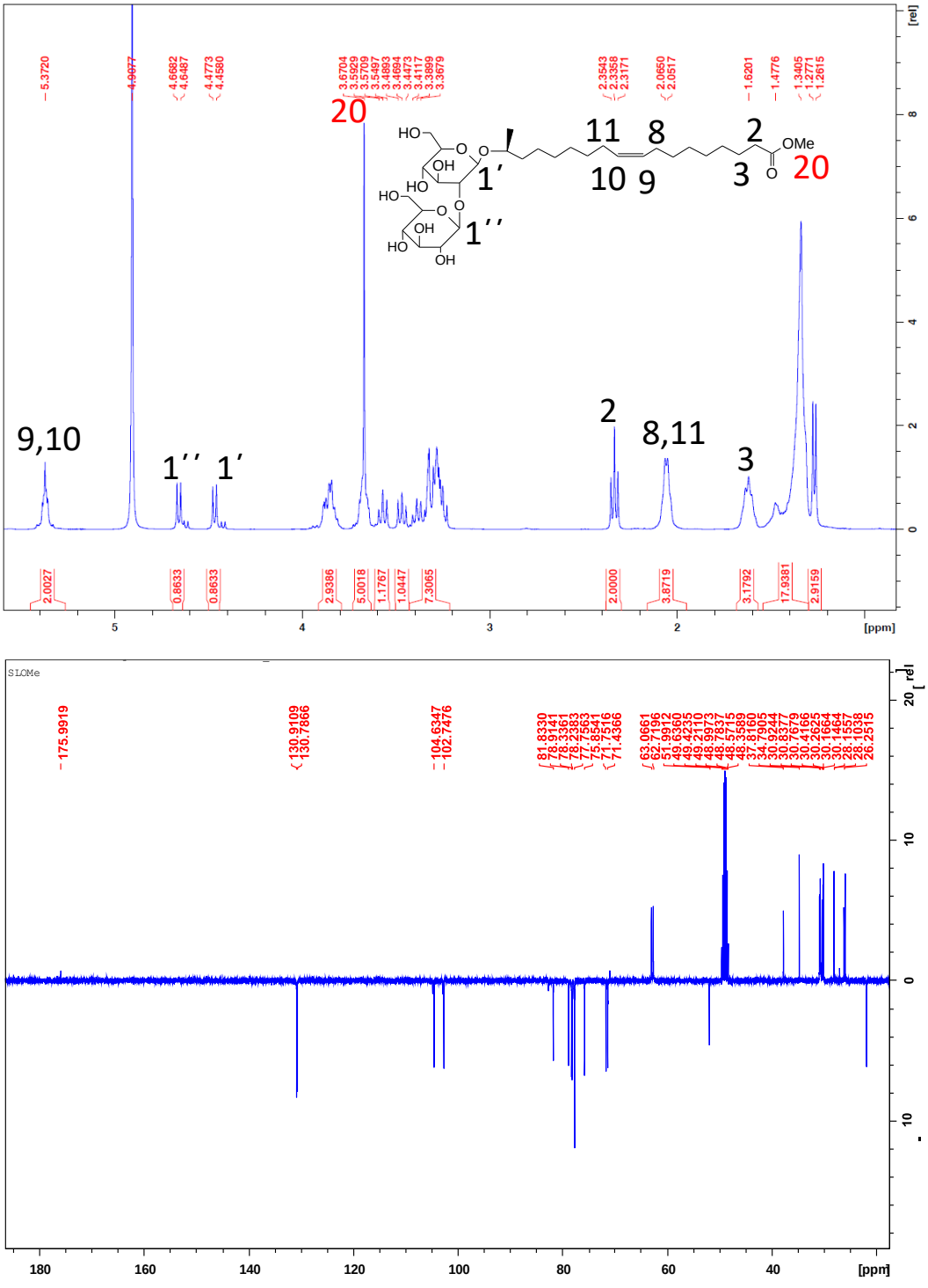

Figure S 2 – ^{1}H and ^{13}C (APT) solution NMR spectrum in MeOD-d4 of monounsaturated aminyl sophorolipid, SL-C18:1-OMe

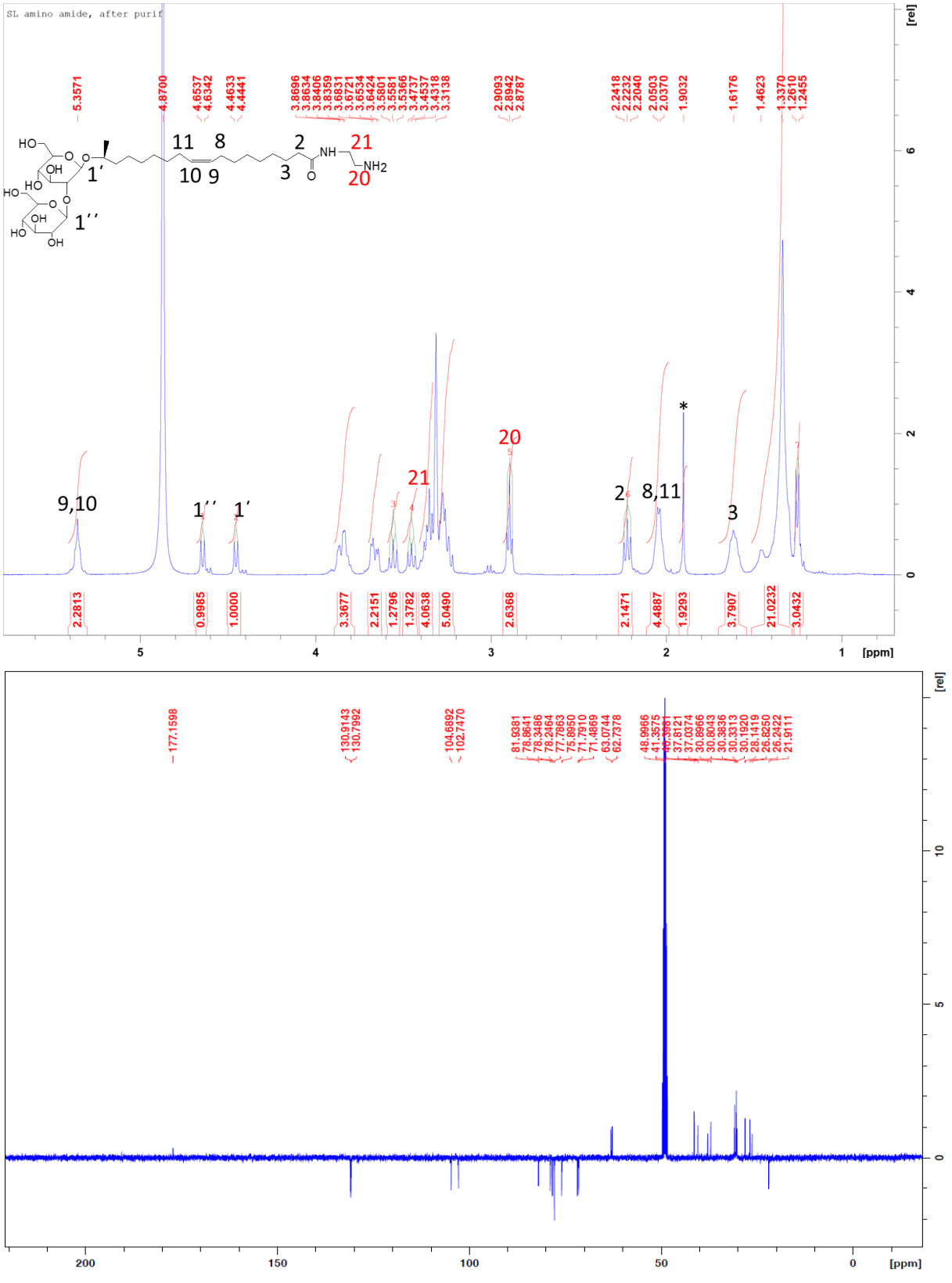

Figure S 3 – ^{1}H and ^{13}C (APT) solution NMR spectrum in MeOD-d4 of monounsaturated aminyl sophorolipid, SL-C18:1-NH_2. The * symbol in the ^{1}H NMR spectrum indicates a contaminant in the NMR tube.

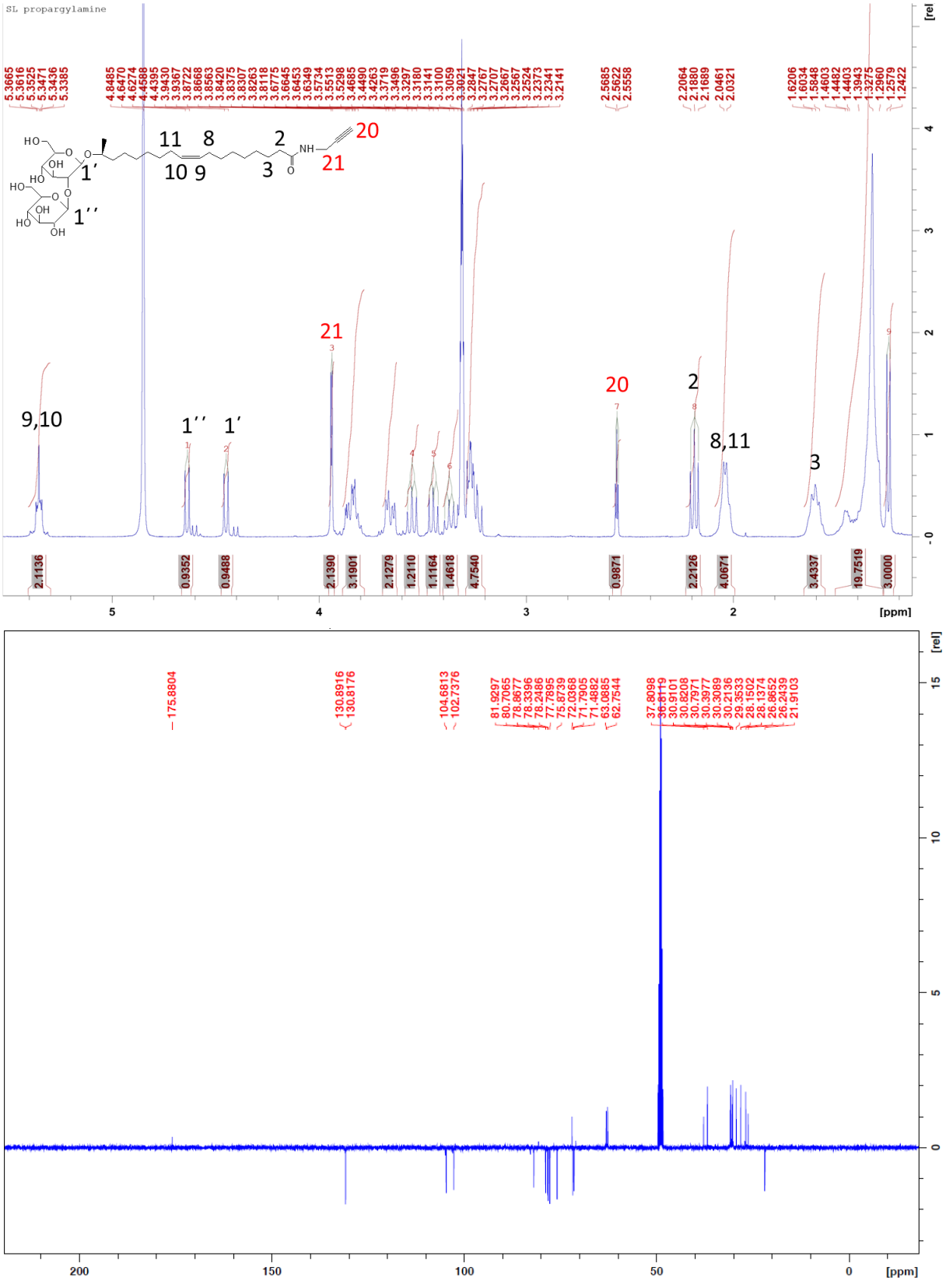

113

114

115 **Figure S 4 - ^{1}H and ^{13}C (APT) solution NMR spectrum in MeOD-d4 of sophorolipid alkynyl, SL-C18:1-**

116 **C≡CH**

117

Small Angle X-ray Scattering (SAXS). SAXS experiments are performed at the DUBBLE BM26B beamline at the ESRF synchrotron facility (Grenoble, France).[6,7] Samples have been analyzed during the run SC4639 using a beam at 11.93 KeV and a sample-to-detector distance of 2.10 m. Samples are analyzed in quartz capillaries of 2 mm in diameter, including a water solution and an empty capillary, respectively used to subtract the background signal and measure the scattering level of water ($I(0)$= 0.016 cm^{-1}) for absolute scale calibration. The signal of the Pilatus 1M 2D detector (172 x 172 μm pixel size), used to record the data, is integrated azimuthally with PyFAI to obtain the $I(q)$ spectrum ($q = {4\pi \sin\theta}/{\lambda}$, where$2\theta$ is the scattering angle) after masking systematically wrong pixels and the beam stop shadow. Silver behenate ($d_{(100)}$ = 58.38 Å) is used as SAXS standard to calibrate the q-scale. Experiments are performed at room temperature (23 ± 2°C) for SL-C18:1-NH_2 and SL-C18:0-NH_2 solutions. The SL-C18:1-C≡CH solution was on the contrary measure both at room temperature and after heating to 90°C. However, considering the fact that the beamline did not dispose of a temperature-controlling unit during beamtime, the 90°C could not be carefully controlled. In practice, the capillary containing the SL-C18:1-C≡CH solution is heated at 90°C for about 5 min, when the solution becomes clear. The capillary is then transferred as fast as possible in front of the beam and the experiment run immediately after. All in all, between removal from the 90°C source and the acquisition we estimate about 2 to 3 min, which could cause a loss in effective temperature of the solution in the capillary of few degrees. Although we cannot guarantee that acquisition occurred when the solution was at 90°C, the solution was still clear during the analysis and no precipitation occurred. To avoid confusion on this point and to indicate that the temperature is not strictly controlled, we employ the notation T= ~90°C when referring to the SAXS experiment in the text.

Small Angle Neutron Scattering (SANS). SANS experiments have been performed at the D11 beamline of Institut Laue Langevin (Grenoble, France). Four q-ranges have been explored and merged using the following wavelengths, λ, and sample-to-detector (StD) distances. 1) ultra-low-q: λ= 13.5Å, StD= 39 m; 2) low-q: λ= 5.3Å, StD= 39 m; 3) mid-q: λ= 5.3Å, StD= 8 m; 4) high-q: λ= 5.3Å, StD= 1.4 m. All samples are prepared in 99.9% D_2O (including the use of using NaOD and DCl solutions for pH change) to limit the incoherent background scattering. Solutions are analyzed in standard 1 mm quartz cells. Direct beam, empty cell, H_2O are recorded and boron carbide (B4C) is used as neutron absorber. The background sample (D_2O) signal was subtracted from the experimental data. Absolute values of the scattering intensity

are obtained from the direct determination of the number of neutrons in the incident beam and the detector cell solid angle. The 2D raw data were corrected for the ambient background and empty cell scattering and normalized to yield an absolute scale (cross section per unit volume) by the neutron flux on the samples. The data were then circularly averaged to yield the 1D intensity distribution, $I(q)$. The software package Grasp (developed at ILL and available free of charge) is used to integrate the data, while the software package SAXSUtilities (developed at ESRF and available free of charge) is used to merge the data acquired at all configurations and subtract the background. Experiments are thermalized at 25°C using the beamline sample temperature controller.

Analysis of the scattering data. SAXS and SANS data were analyzed using a model-dependent and model-independent approach. The low-q region below $q < 0.2$ nm^{-1} is analyzed using a classical evaluation of the slope of $I(q)$ in a log-log scale. The data are fitted using a linear function, of which the slope is generally related to a specific morphology (e.g., -1: cylinders; -2: lamellae),[8] or it describes the presence of fractal objects.[9] The region between $\sim 0.2 < q$ / nm^{-1} $< \sim 5$ is analyzed with both model-independent (Guinier) and model-dependent (core-shell prolate ellipsoid of revolution form factor) functions.

The model-independent Guinier analysis can be safely applied to those data showing a plateau below $q < 0.2$ nm^{-1}.[8] Within the Guinier approximation $q.R_g < 1$, with q being the wavevector and R_g the radius of gyration, the scattered intensity can be approximated by

$$I(q) = I_0 e^{-\frac{R_g^2 q^2}{3}}$$

which, expressed in the log-log plot, gives

$$Log(I) = Log(I_0) - \frac{Log(e) R_g^2}{3} q^2 = a + bq^2.$$

R_g is obtained by linearization and plotting $Log(I)$ against q^2, with the slope being equal to $b = -0.434 \frac{R_g^2}{3}$, with $Log(e) = 0.434$. For a spherical object, one can estimate the radius of the corresponding sphere, R, according to

$$R_{Guinier} = \sqrt{\frac{5}{3} R_g^2} = \sqrt{5 \cdot (-\frac{b}{0.434})}$$

The error on $R_{Guinier}$ is derived from the error of the linear fit.

The model-dependent analysis consists in employing a core-shell (prolate) ellipsoid of revolution form factor model with inhomogeneous shell thickness, also referred to as the

"*coffee-bean*" model, in agreement with previous modelling of SAXS data recorded on deacetylated acidic C18:1 sophorolipids.[10,11] The model is implemented in the SasView 3.1.2 software (CoreShellEllipsoidXT),[a] the general equation of which is

$$I(q) = \frac{scale}{V}(\rho - \rho_{solv})^2 P(q) S(q) + bkg$$

where, $scale$ is the volume fraction, V is the volume of the scatterer, ρ is the Scattering Length Density (SLD) of the object, ρ_{solv} is the SLD of the solvent, $P(q)$ is the form factor of the object, bkg is a constant accounting for the background level and $S(q)$ is the structure factor, which is hypothesized as unity in the analyzed range of q-values and at the present concentrations. The analytical expression of $P(q)$ for a core-shell ellipsoid of revolution model implemented in the software is provided on the developer's website[a], while Figure S 5 shows the geometrical model, where T is the equatorial shell thickness, T_1 is the polar shell thickness, R, the equatorial core radius, R_1, the polar core radius. The model implies the evaluation of ρ_{core}, ρ_{shell}, ρ_{solv}, the SLDs of, respectively, the hydrophobic core, hydrophilic shell and solvent. The model also considers a non-homogeneous core and shell, for we define the aspect ratio of the core and shell respectively being $\frac{R_1}{R}$ and $\frac{T_1}{T}$. The SLD can be calculated using the SLD calculator implemented in the SasView 3.1.2 software and based on

$$\rho = \frac{\sum_i^j Z_i r_e}{v_M}$$

where Z_i is the atomic number of the i^{th} of j atoms in a molecule of molecular volume v_M, r_e is the classical electron radius or Thomson scattering length (2.8179×10^{-15} m). The list of fixed and variable in our approach is given in Figure S 5

[a] http://www.sasview.org/sasview/user/models/model_functions.html#coreshellellipsoidxtmodel

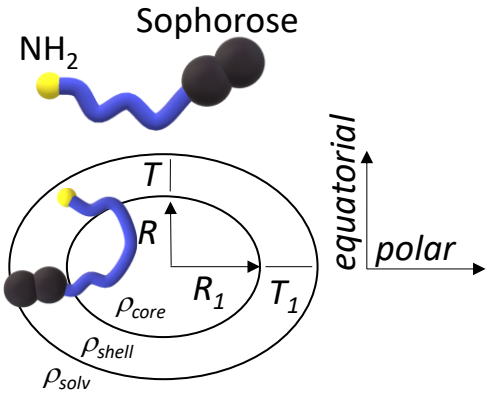

Parameter	Value
T	Variable
T_1/T	Variable
R	Variable
R_1/R	Variable
ρ_{shell}	Variable
ρ_{core}	8.4×10^{-4} nm^{-2}
ρ_{solv}	9.4×10^{-4} nm^{-2}

Figure S 5 – The "*coffee-bean*" micellar model: core-shell prolate ellipsoid of revolution form factor model with inhomogeneous shell thickness ($T_1 \neq T$) adapted from Ref. [10,11] and available in the SasView 3.1.2 software (CoreShellEllipsoidXTModel).[a] List of the main fixed and variable parameters used in the model to fit the SAXS data.

The values of 8.4 and 9.4 x 10^{-4} nm^{-2}, respectively for ρ_{core} and ρ_{solv}, are typical for a hydrocarbon chain in sophorolipids[11] and for water. ρ_{shell} accounts for the carbohydrate moieties, water and counterions, and it is always a variable parameter, although it should be contained between the hydrated and dehydrated sophorose, that is between 10.0 and 14.0 x 10^{-4} nm^{-2}.[11] If the overall quality of the fit can be followed by the classical χ^2 evolution test, a realistic estimation of the error on the final values is always difficult, although an error of ±10% is not outrageous. In our fitting strategy, the starting best-fit parameters are determined on the basis of previous work;[10] R, T and ρ_{shell} are then varied keeping $\frac{R_1}{R} = \frac{T_1}{T} = 1$. The fit is then refined by varying $\frac{R_1}{R}$ and $\frac{T_1}{T}$ independently.

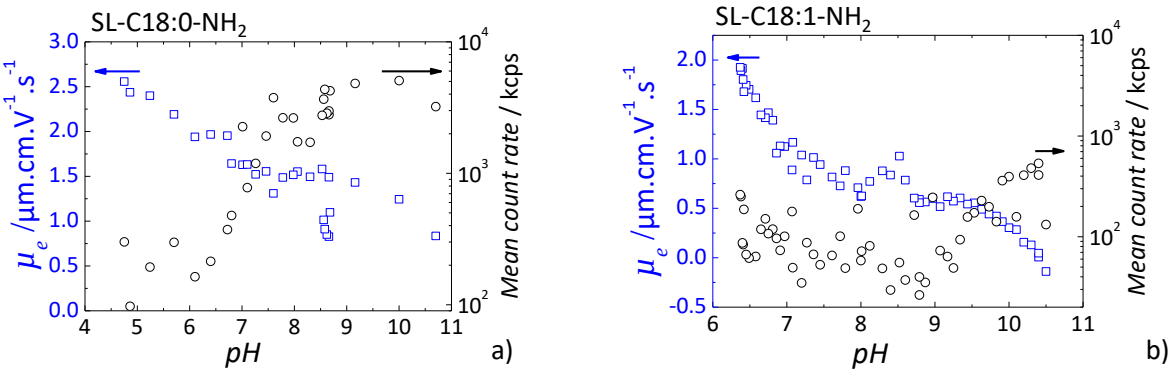

Figure S 6 – Electrophoretic mobility (blue empty squares) and turbidimetric (black empty circles) experiments performed on a) SL-C18:0-NH_2 (C= 2 mg/mL) and b) SL-C18:1-NH_2 (C= 5 mg/mL) solutions. The experimental conditions are given in the materials and method section.

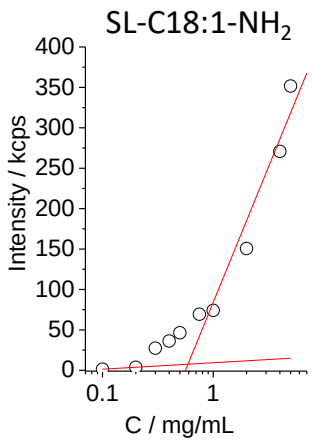

CMC= 0.5 ± 0.2 mg/mL

Figure S 7 – Critical micelle concentration study of aminyl sophorolipid SL-C18:1-NH_2 using static light scattering at constant shutter opening.

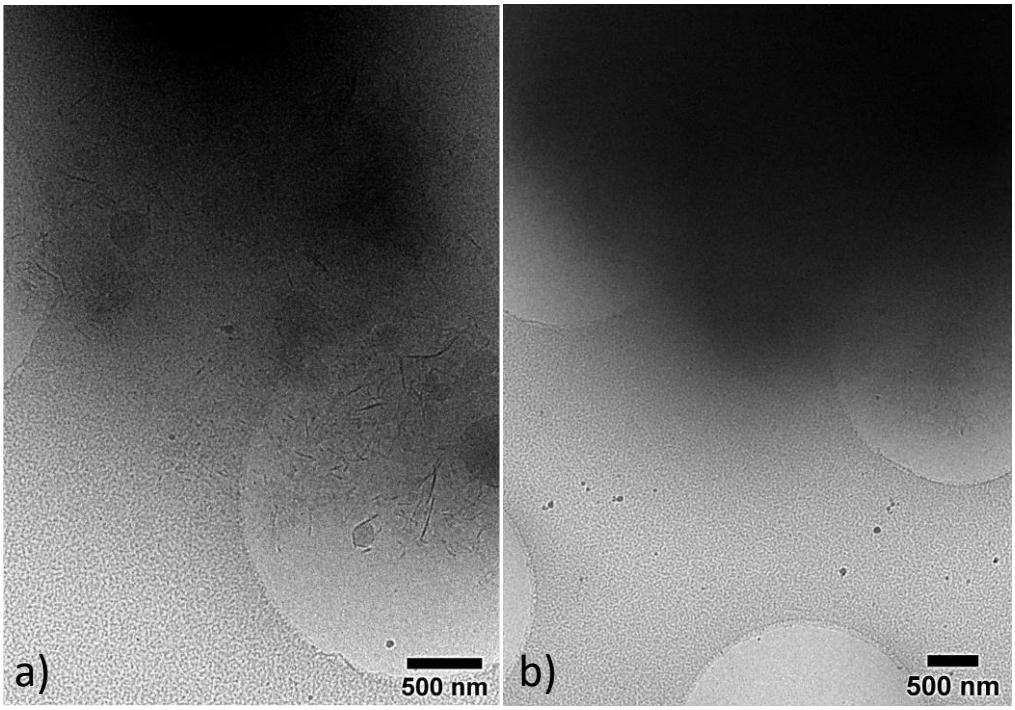

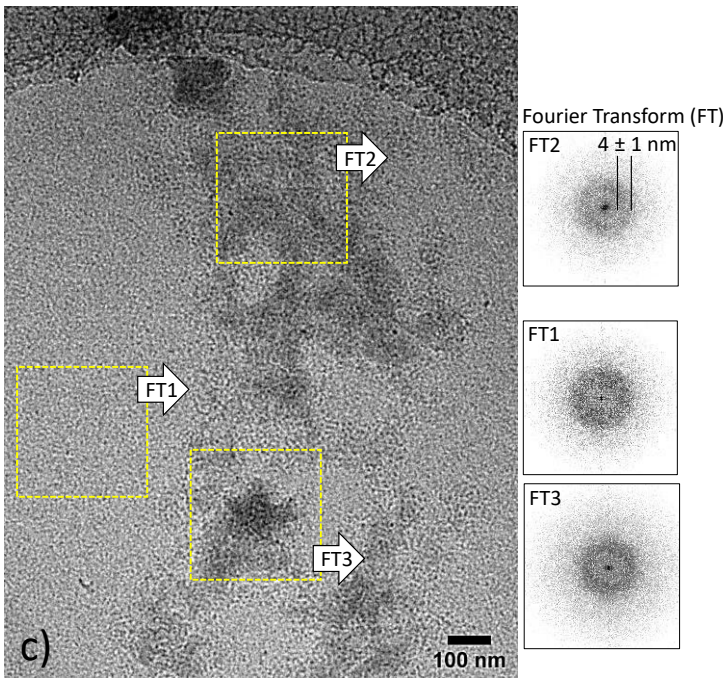

Figure S 8 – Highlight of the micellar region in cryo-TEM experiments performed on a SL-C18:1-NH_2 solution at C= 0.5 wt% and pH 4. a-b) Typical visual look of cloudy regions corresponding to aggregated platelets. These are sitting on top of the holey carbon grid, where holes contain vitrified water. c) Close-up of a vitrified aqueous hole in another region of the same grid. Micellar aggregates are visible within the vitrified layer of water. The Fourier Tranform (FT) corresponding to the yellow highlights are given on the right-hand side. The broad scattering ring identifies a correlation distance of 4 ± 1 nm, in agreement with the micellar diameter measured by SAXS.

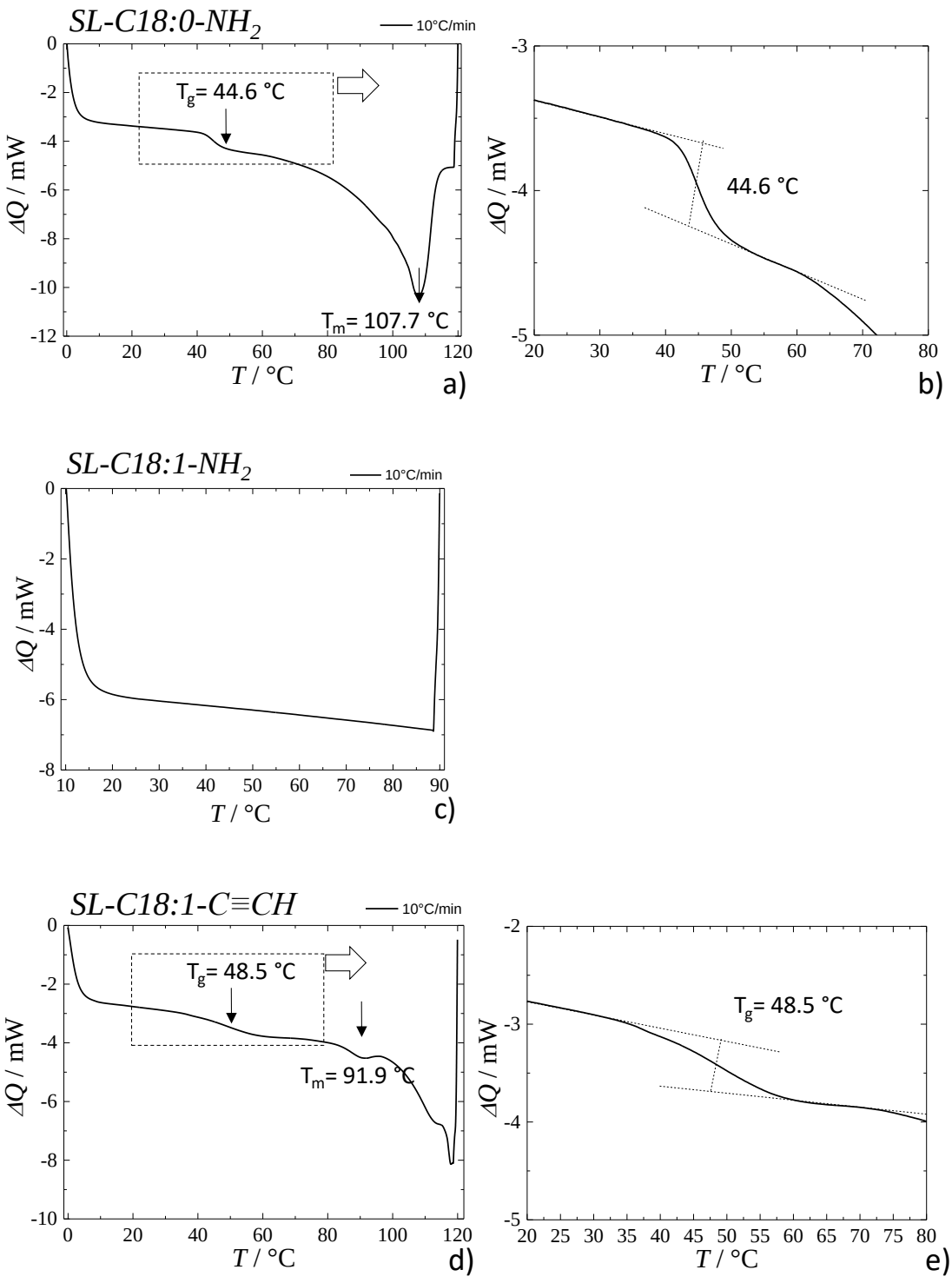

Figure S 9 – DSC experiments performed on SL-C18:0-NH_2, SL-C18:1-NH_2 and SL-C18:1-C≡CH powder samples at heating rate of 10°C/min. Error on the value of T_g is estimated to be ± 0.5°C and it is related to the uncertanty associated to the tangets method. The value of T_m is determined by fitting the profile with a Lorentzian peak.

References

1 E. I. P. Delbeke, B. I. Roman, G. B. Marin, K. M. Van Geem and C. V. Stevens, *Green Chem.*, 2015, **17**, 3373–3377.

2 P. K. Singh, R. Mukherji, K. Joshi-Navare, A. Banerjee, R. Gokhale, S. Nagane, A. Prabhune and S. Ogale, *Green Chem.*, 2013, **15**, 943–953.

3 K. S. Bisht, R. A. Gross and D. L. Kaplan, *J. Org. Chem.*, 1999, **64**, 780–789.

4 A.-S. Cuvier, J. Berton, C. V Stevens, G. C. Fadda, F. Babonneau, I. N. a Van Bogaert, W. Soetaert, G. Pehau-Arnaudet and N. Baccile, *Soft Matter*, 2014, **10**, 3950–9.

5 N. Baccile, M. Selmane, P. Le Griel, S. Prévost, J. Perez, C. V. Stevens, E. Delbeke, S. Zibek, M. Guenther, W. Soetaert, I. N. A. Van Bogaert and S. Roelants, *Langmuir*, 2016, **32**, 6343–6359.

6 G. Portale, D. Cavallo, G. C. Alfonso, D. Hermida-Merino, M. van Drongelen, L. Balzano, G. W. M. Peters, J. G. P. Goossens and W. Bras, *J. Appl. Crystallogr.*, 2013, **46**, 1681–1689.

7 W. Bras, I. P. Dolbnya, D. Detollenaere, R. van Tol, M. Malfois, G. N. Greaves, A. J. Ryan and E. Heeley, *J. Appl. Crystallogr.*, 2003, **36**, 791–794.

8 O. Glatter and O. Kratky, *Small Angle X-ray Scattering*, Academic Press, London, 1982.

9 J. Teixeira, *J. Appl. Crystallogr.*, 1988, **21**, 781–785.

10 N. Baccile, A.-S. Cuvier, S. Prévost, C. V Stevens, E. Delbeke, J. Berton, W. Soetaert, I. N. A. Van Bogaert and S. Roelants, *Langmuir*, 2016, **32**, 10881–10894.

11 S. Manet, A. S. Cuvier, C. Valotteau, G. C. Fadda, J. Perez, E. Karakas, S. Abel and N. Baccile, *J. Phys. Chem. B*, 2015, **119**, 13113–13133.